J Mater Sci (2010) 45:2317–2323
DOI 10.1007/s10853-009-4195-z

Effect of Pb doping on structural and electrochemical properties of combustion synthesised $LiCoO_2$ powder

S. Valanarasu · R. Chandramohan

Received: 1 September 2009 / Accepted: 31 December 2009 / Published online: 20 January 2010

Abstract Pb-doped $LiCoO_2$ cathode materials, containing 0–10 mol% of Pb were synthesised by the starch-assisted combustion technique. X-ray diffraction analyses revealed the existence of rhombohedral $LiCoO_2$ (*R-3m*) for all compounds. Scanning electron microscopy showed a distinct grain growth with increasing Pb content. The synthesised samples are characterised using X-ray photoelectron spectra (XPS), to investigate the elementary states on the system. The electrical conductivity of Pb-doped $LiCoO_2$ system tends to increase with Pb content significantly. Decrease of the electrode impedance was observed with increase in Pb content in system. An excellent reversible capacity was observed for the cathode containing 5.0 mol% Pb, when 2016 type coin cells were cycled at 0.1 C rate. This has been ascribed to the structural stability induced by Pb doping.

Introduction

Lithium cobalt oxide ($LiCoO_2$) is the most widely used cathode material for lithium-ion batteries due to its superior electrochemical performance in terms of high discharge capacity (120–160 $mAhg^{-1}$) and excellent cycleability ($\sim$1000 cycles) compared to other cathodes known so far [1–6]. However, the practically achieved capacity is only $\sim$50% of its theoretical capacity ($\sim$273 $mAhg^{-1}$) because the amount of Li that can be extracted is limited to only 0.5 mol/mol of $LiCoO_2$, beyond which the layered rhombohedral structure collapses and gives way to an electrochemically inactive monoclinic phase. Transition and non-transition elements, e.g. Ti [7], Cr [8], Mn [9], Ni [10], Fe [11], Cu [12], Bi, Zr, Sn [13], Zn [12], Mo, V [14] have been studied extensively as dopants in $LiCoO_2$ with the aim of improving its electrochemical characteristics in terms of cycling efficiency, intercalation voltage and cost reduction. Though Pb is toxic, its mean value of toxicity is lower than Co [15]. Thus, the addition of Pb reduces the net toxicity of the system. Also, Pb is reported to be doped into some superconductor materials to increase the carrier concentration and the enhancement of the electrical conductivity [16]. Because of the homogeneous distribution and good connectivity between the grains in Pb-doped samples an improvement in electrical conductivity can be expected and may help in the electronic charge transfer during Li intercalation–deintercalation [17]. Hence Pb doping may result in improved conductivity and structural stability in $LiCoO_2$ system. To the best of our knowledge, no study has been made on the Pb-doped $LiCoO_2$ cathode material so far. Thus, in the present work, we report on the synthesis of Pb-doped $LiCoO_2$ powder by combustion technique. The influence of Pb on the material properties are discussed and correlated to the electrochemical properties of these cathode materials.

Experimental

For the synthesis of Pb-doped $LiCoO_2$ powders (0–10 mol% of Pb), a combustion route was adopted and the procedure is shown in Fig. 1. Calculated amount (2 g) of 'water soluble' starch was dissolved in 20 mL of hot distilled water. To the hot starch solution was added stoichiometric amount of

S. Valanarasu
Physics Department, Ananda College, Devakottai 630303, India

R. Chandramohan (✉)
Physics Department, Sree Sevugan Annamalai College, Devakottai 630303, India
e-mail: chandru17@yahoo.com

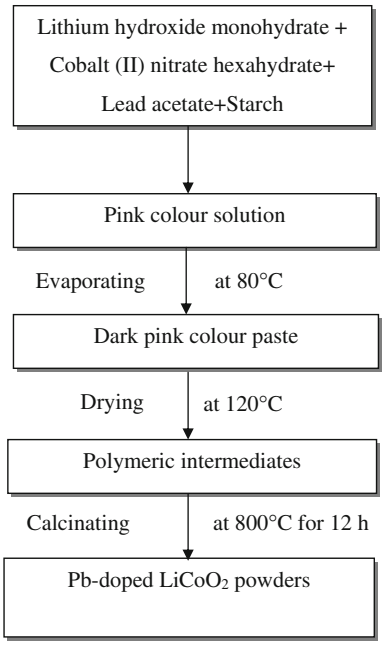

Fig. 1 Schematic of starch assisted combustion process for the synthesis of Pb-doped $LiCoO_2$ powders

lithium hydroxide monohydrate ($LiOH{\cdot}H_2O$), cobalt (II) nitrate hexahydrate ($Co(NO_3)_2{\cdot}6H_2O$) and lead acetate $Pb(CH_3COO)_2$ solutions that were (metal ions ratio Li:Pb:Co is $1{:}x{:}1-x$) mixed with starch solution. The obtained pink colour solution was evaporated at 80 °C for 6 h with constant stirring. Continuous evaporation leads to the formation of a dark pink coloured polymeric resin. The polymeric resin was further dried at 120 °C for 12 h to remove the excess water, which led to the formation of a solid mass. Subsequently, these intermediates were heat treated at 800 °C for 12 h. Unlike glycine, a molar correlation in terms of a chemical equation may not be possible in the case of starch. Being a polysaccharide $(-C_6H_{10}O_5-)_n$ starch does not have a definite n value [18].

The crystalline structure was determined by X-ray diffraction using X'pert PRO (PANalytical) diffractometer with Cu Kα radiation ($\lambda = 0.15405$ nm) and employing scanning rate of 5° min^{-1} over the 2θ range of 15°–75°. The particle size and morphology was examined using scanning electron microscope (SEM) Hitachi S-3000H model. For SEM studies the samples are coated with Au using JFC-1100 model instrument. XPS measurements were made using a LAS-3000 surface analysis system and Al Kα X-rays (1489.6 eV, width 0.5 eV). The electrical conductivity was measured by a two probe method from room temperature to 150 °C uniformly on circular pellets of diameter of ~10 mm and thickness of ~2 mm. The impedance spectra were recorded using a Schlumber 610 electrochemical interface and frequency response analyzer. The frequency range was 0.001 Hz to 100 kHz and the amplitude of the perturbation signal was 30 mV. The electrochemical performance was studied by assembling 2016 coin-type cells. Cathodes were prepared from a slurry of the synthesised Pb-doped $LiCoO_2$ powder (80%), acetylene black (10%) and (polyvinylidene fluoride) PVDF binder (10%) in n-methyl pyrrolidinone (NMP) solvent. The slurry was coated on an aluminium foil (current collector) and was dried at 110 °C in an oven for 12 h. It was then pressed under a pressure of 4 tonne $inch^{-2}$ for 1 min. Finally, circular discs of 18 mm diameter were cut and used as cathodes. The cells were assembled using Li metal as anode and $LiPF_6$ in EC:DMC (1:1 vol.%) as electrolyte within an argon-filled glove box. Galvanostatic discharge studies were carried out at a current rate of 0.1 C.

Results and discussions

Figure 2 shows the X-ray diffractograms for pristine $LiCoO_2$ (Pb0), 1 mol% (Pb1), 3 mol% (Pb3), 5 mol% (Pb5) and 10 mol% (Pb10) of Pb-doped $LiCoO_2$ samples. For all samples, the characteristic peaks of a standard rhombohedral $LiCoO_2$ can be identified (JCPDS File No. 75-0532). The characteristic splitting of the (0 0 6)/(0 1 2)

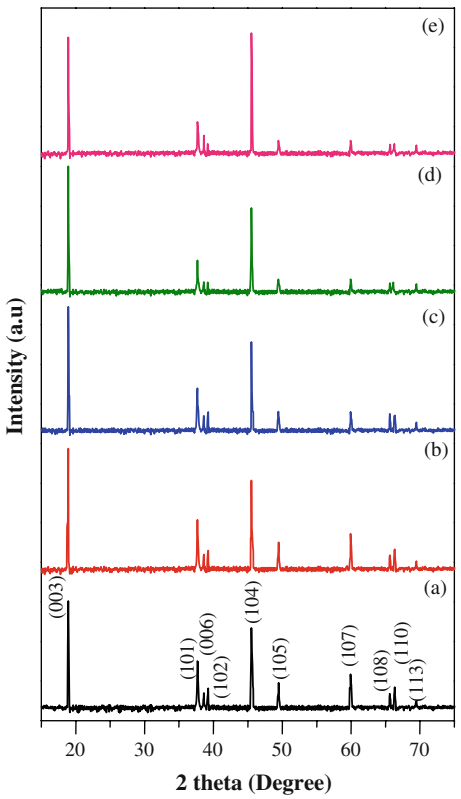

Fig. 2 X-ray diffraction patterns of the Pb-doped $LiCoO_2$. (*a*) Pristine $LiCoO_2$ (Pb0), (*b*) 1 mol% (Pb1), (*c*) 3 mol% (Pb3), (*d*) 5 mol% (Pb5) and (*e*) 10 mol% (Pb10)

peaks and (0 1 8)/(1 1 0) peaks suggests that the ordered array of cobalt and oxygen atoms remains unperturbed even after the addition of Pb into the $LiCoO_2$ matrix. The lattice parameters of the synthesised powders were calculated for (003) and (104) planes. As shown in Table 1, both the lattice parameters *a* and *c* increase upon Pb doping, although no systematic change is observed. The lattice parameter, *a*, indicates the metal–metal intralayer distance while *c* represents the interlayer spacing [17]. Lattice substitution by elements with larger ionic radii often leads to expansion of the unit well parameters. Thus, considering the large difference in ionic radii of Pb^{2+} ($\sim$0.132 nm) compared Co^{3+} ($\sim$0.063 nm), the observed increase in *a* and *c* values in Pb-doped $LiCoO_2$ can be explained. The intensity ratio value $I_{(0\ 0\ 3)}/I_{(1\ 0\ 4)}$ increases with increasing molar concentration in Pb-doped $LiCoO_2$ and decreases to

Table 1 The lattice parameters of Pb-doped $LiCoO_2$ powders

Sample code	*d* (Å)	*a* (Å)	*c* (Å)	*c*/*a*	$I_{(0\ 0\ 3)}/I_{(1\ 0\ 4)}$
Pb0	4.676	2.841	14.027	4.94	1.29
Pb1	4.680	2.853	14.039	4.92	1.31
Pb3	4.681	2.867	14.043	4.89	1.34
Pb5	4.683	2.869	14.049	4.89	1.43
Pb10	4.687	2.893	14.061	4.86	0.98

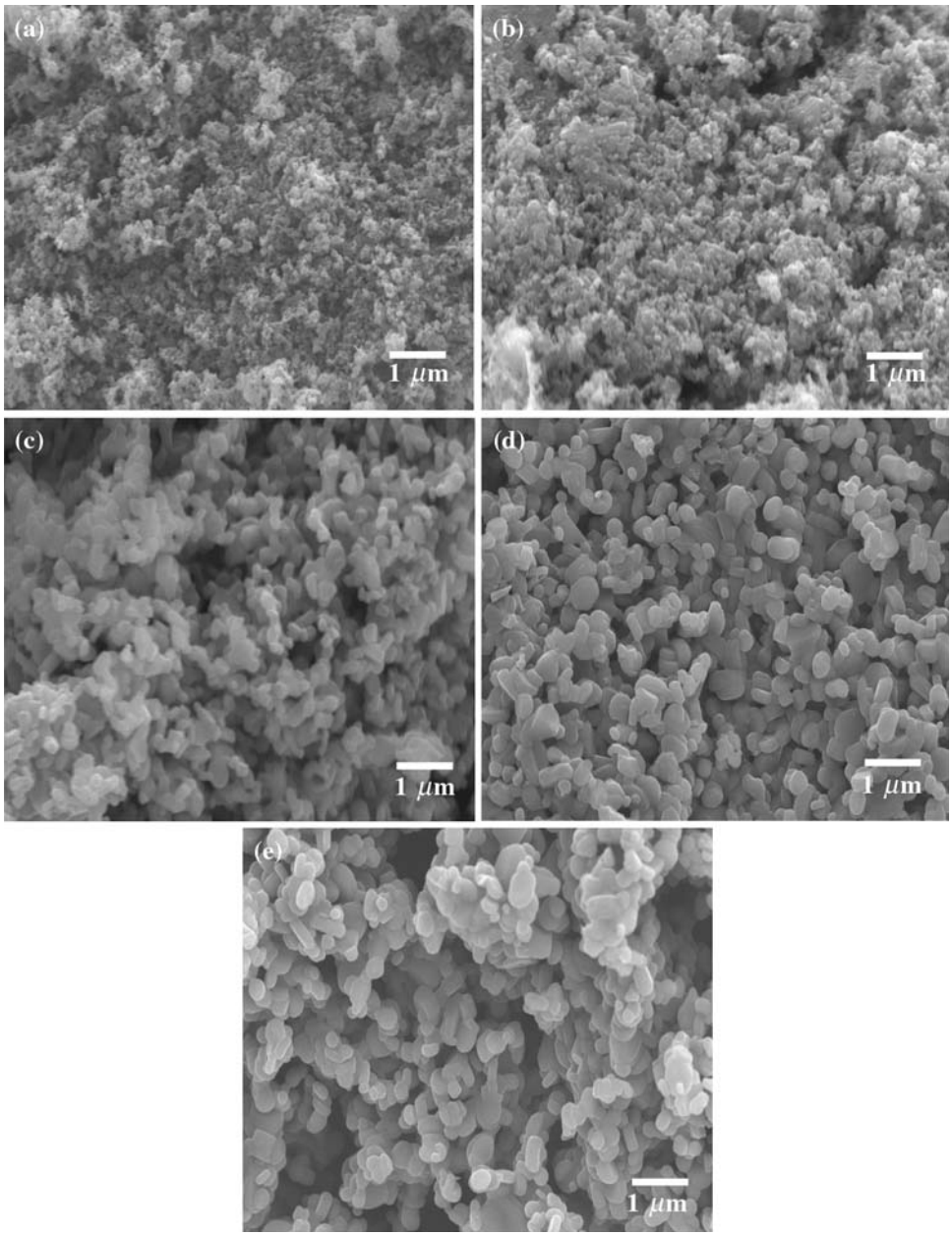

Fig. 3 SEM image of the Pb-doped $LiCoO_2$ powders synthesised at 800 °C. **a** Pristine $LiCoO_2$ (Pb0), **b** 1 mol% (Pb1), **c** 3 mol% (Pb3), **d** 5 mol% (Pb5) and **e** 10 mol% (Pb10)

0.98 for 10 mol%, less than the critical value of 1.2 [19], suggesting that cation mixing happens at higher doping level (Pb10).

Figure 3a–e shows the SEM images of pristine $LiCoO_2$ (Pb0) and Pb-doped $LiCoO_2$ (Pb1, Pb3, Pb5 and Pb10), respectively. A partially agglomerated mass of $LiCoO_2$ grains can be seen in the micrographs of all the samples. Spherically shaped grains measuring approximately 10–100 nm are observed for pristine $LiCoO_2$ (Pb0). Morphological change occurs when Pb is added in the matrix of $LiCoO_2$ as is revealed in Fig. 3b. The increase of grain size is observed for Pb1, that lies in the range 50–150 nm. The grain size increases further for Pb3 (100–200 nm) with some voids. Good electrical contact between the grains has been observed for $LiCoO_2$ (Pb5) with grain size of 200–300 nm. The SEM micrographs of a Pb10 exhibit two features. One feature corresponding to spherical grains of diameter around 250 nm and the other corresponds to elliptical shaped grains around 400 nm mean diameter.

X-ray photoelectron spectroscopy (XPS) is known for the study of the composition and binding energy. Figure 4a shows the wide-scan spectra of the 10 mol% (P10) of Pb-doped $LiCoO_2$ in the range of 0–1200 eV. Figure 4b–e shows the enlarged regions of the XPS spectra of the hexagonal 10 mol% (P10) of Pb-doped $LiCoO_2$. In the energy range 770–820 eV, peaks due to Co $2p_{3/2}$ at 780 eV and Co $2p_{1/2}$ at 796 eV are observed. Similarly in the energy range 50–80 eV, peaks due to Li 1s at 54.5 eV, Co

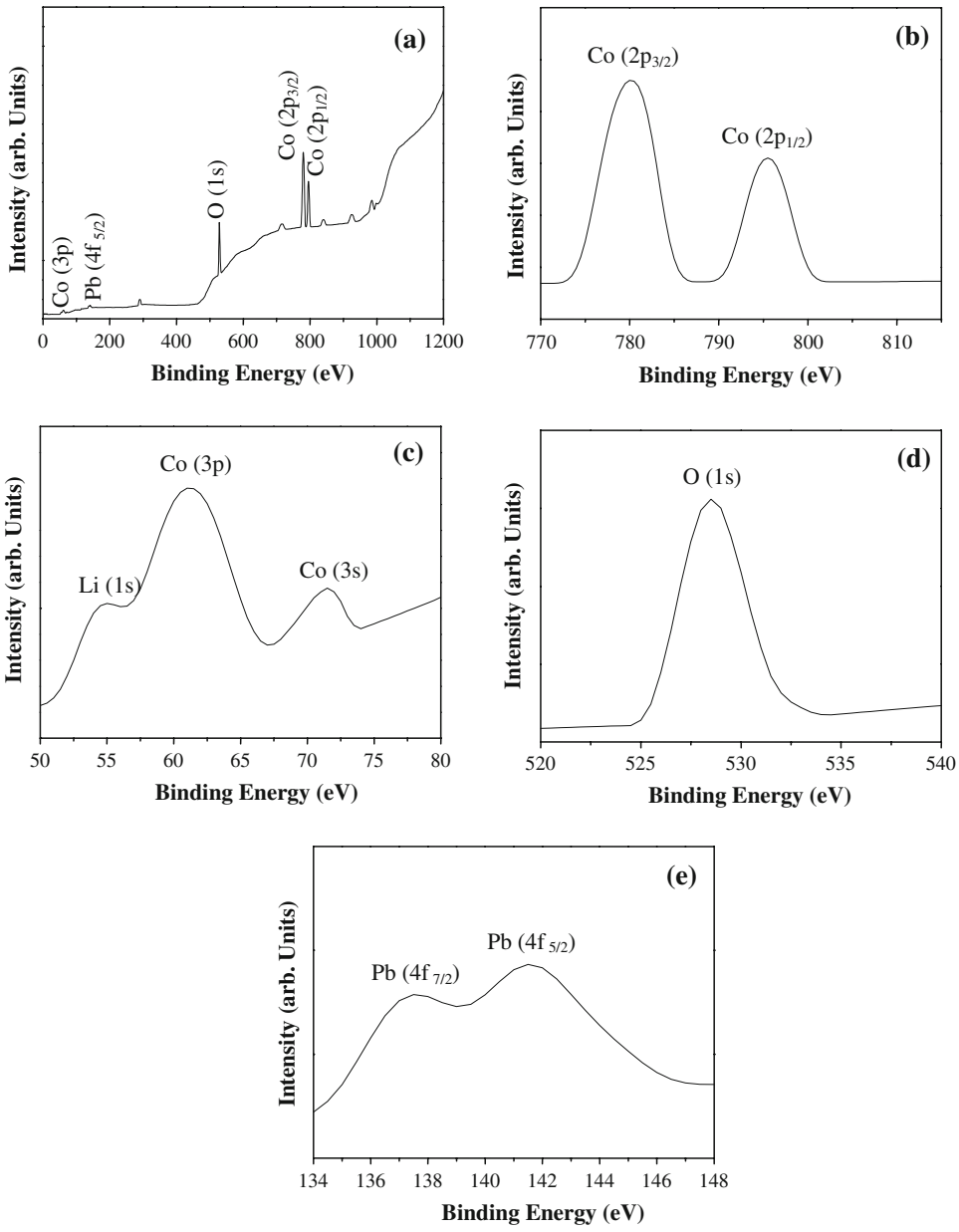

Fig. 4 XPS spectra of **a** a complete XPS spectra of $LiCo_{0.90}Pb_{0.1}O_2$ sample, **b** Co, ($2p_{3/2}$) and Co ($2p_{1/2}$), **c** Li (1s), Co (3p) and Co (3s), **d** oxygen (1s), **e** Pb ($4f_{7/2}$) and Pb ($4f_{5/2}$)

3p at 61 eV and Co 3s at 71 eV are observed. In the energy range 520–540 eV a peak corresponding to O 1s at 529 eV is observed. In the energy range 134–148 eV, peaks due to Pb $4f_{7/2}$ at 136.8 eV and Pb $4f_{5/2}$ at 141.9 eV, respectively, are observed. The results are in good agreement with the literature [20, 21].

The electronic conductivity is a very important property of a cathode material. For a better charge transfer process during lithium intercalation–deintercalation in lithium-ion cells, conductivity plays a significant role [22, 23]. Figure 5 shows the electrical conductivity of Eu-doped $LiCoO_2$ system measured from room temperature to 150 °C. The room temperature conductivity of pristine $LiCoO_2$ is found to be 1.2×10^{-4} Scm^{-1}. All the Pb-doped compounds show higher room temperature conductivity with respect to pristine $LiCoO_2$. The conductivity increases with increasing amount of Pb per mole of $LiCoO_2$. A conductivity value of 4.6×10^{-2} Scm^{-1} is observed for 10 mol% which is about two orders of magnitude higher than pristine $LiCoO_2$.

The ac impedance spectra of the Pb-doped $LiCoO_2$/Li cells at their fully charged state (about 4.5 V) after 30 cycles are shown in Fig. 6. Obviously, as a result of Pb doping, the cell impedance decreases substantially. Considering the fact that all these cells use the same Li electrode and electrolyte, the difference should be dominantly contributed from the cathode (Pb–$LiCoO_2$ side). Assuming the equivalent circuit of this cathode impedance is similar to the case of $LiNi_{0.8}Co_{0.2}O_2$/Li cells [24], the high frequency semicircle and the intermediate frequency semicircle on these spectra are associated with the surface film resistance (R_{sf}) and charge transfer resistance (R_{ct}) on the cathode side, respectively. Thus, it can be seen from Fig. 6 that both R_{sf} and R_{ct} decrease with increasing the Pb doping level. The surface film resistance (R_{sf}) of Pb0 is found to be

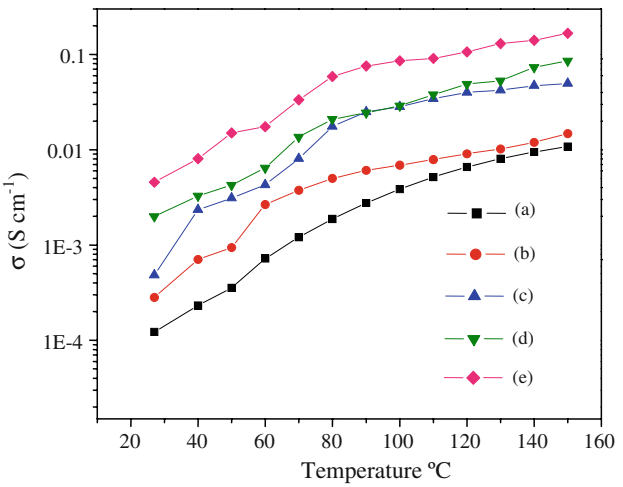

Fig. 5 Electrical conductivity profiles of Pb-doped $LiCoO_2$. (*a*) Pristine $LiCoO_2$ (Pb0), (*b*) 1 mol% (Pb1), (*c*) 3 mol% (Pb3), (*d*) 5 mol% (Pb5) and (*e*) 10 mol% (Pb10)

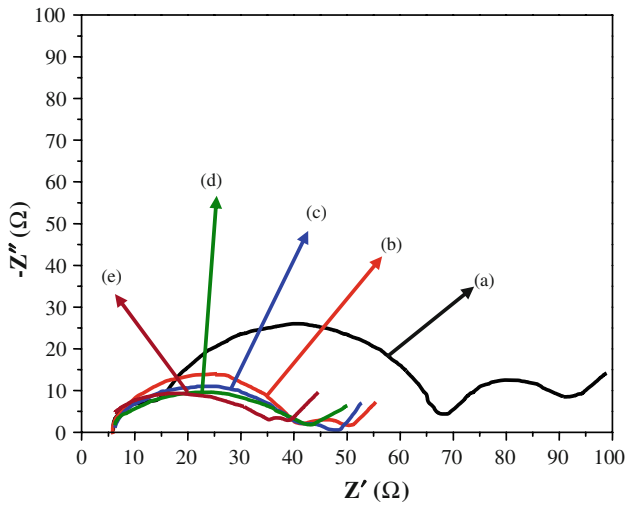

Fig. 6 Electrochemical impedance spectra of Pb-doped $LiCoO_2$/Li cells at 4.5 V of the open circuit voltage: (*a*) pristine $LiCoO_2$ (Pb0), (*b*) 1 mol% (Pb1), (*c*) 3 mol% (Pb3), (*d*) 5 mol% (Pb5) and (*e*) 10 mol% (Pb10)

11 Ω after 30 cycles. On the other hand, both Pb1 and Pb3 show very little change in the surface film resistance. For Pb5, R_{sf} is 6 Ω while for Pb10, it decreases to 5 Ω. Being highly mobile it is probable that Pb would move over to the $LiCoO_2$ surface and form a protective thin layer during Li intercalation–deintercalation. Due to this protective layer, Co dissolution into the acidic electrolyte is prevented to a considerable extent and may stabilise the layered structure. Decrease in impedance in Pb-doped sample may be due to decrease of degradation of the cathode during cycling process.

Figure 7a–e shows the galvanostatic discharge curves of pristine $LiCoO_2$ (Pb0) and Pb–$LiCoO_2$ (Pb1, Pb3, Pb5 and Pb10), respectively. These experiments were carried out at the voltage range of 3.0–4.5 V and the current density 0.1 mAg^{-1} employing current rate of 0.1 C. The first discharge capacity was measured for all the materials and they are 199, 193, 190, 189 and 186 $mAhg^{-1}$ for Pb0, Pb1, Pb3, Pb5 and Pb10 of Pb–$LiCoO_2$ samples, respectively. The decrease in capacity from the first discharge capacity to that in 30th cycle are 34, 22, 16, 09 and 19 $mAhg^{-1}$, respectively for Pb0, Pb1, Pb3, Pb5 and Pb10 of Pb-doped $LiCoO_2$ samples and are shown in Fig. 8. This may be due to the increasing Pb content which effectively reduces the amount of active $LiCoO_2$, resulting in a decrease in the discharge capacity. The capacity fading rate f_c, is defined as

$$f_c = \frac{C_1 - C_n}{n} \quad (1)$$

where C_1 and C_n are the specific discharging capacities of first and *n*th cycle, and *n* is the number cycles. The capacity fading rates are 1.36, 0.88, 0.64, 0.36 and 0.76 $mAhg^{-1}$, respectively, per cycle for Pb0, Pb1, Pb3, Pb5 and Pb10 of

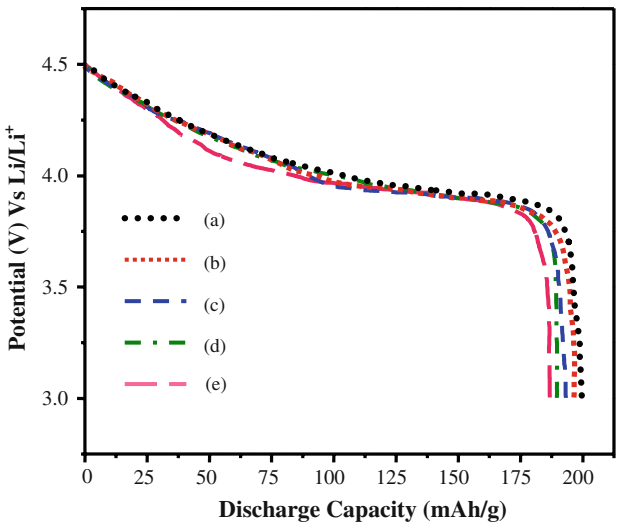

Fig. 7 Typical initial discharge capacity of the Pb-doped $LiCoO_2$. (*a*) Pristine $LiCoO_2$ (Pb0), (*b*) 1 mol% (Pb1), (*c*) 3 mol% (Pb3), (*d*) 5 mol% (Pb5) and (*e*) 10 mol% (Pb10)

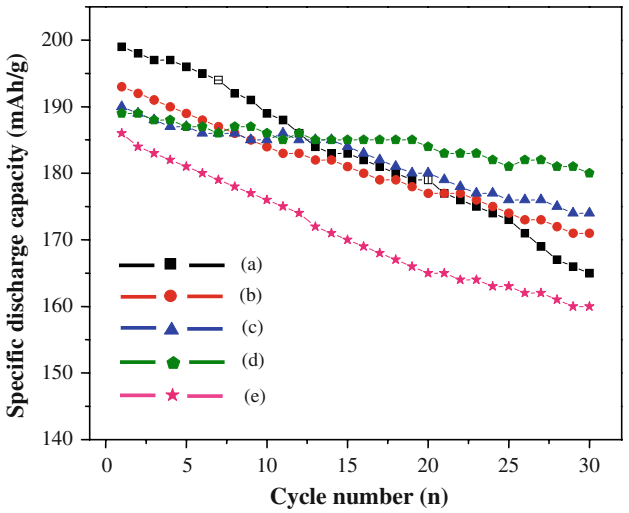

Fig. 8 Plots of specific discharge capacity versus cycle number of Pb-doped $LiCoO_2$. (*a*) Pristine $LiCoO_2$ (Pb0), (*b*) 1 mol% (Pb1), (*c*) 3 mol% (Pb3), (*d*) 5 mol% (Pb5) and (*e*) 10 mol% (Pb10)

Pb-doped $LiCoO_2$ samples. The capacity fading rate decreases first with increase in Pb content up to 5 mol% Pb and then increases with Pb content 10 mol% (Pb10). The above results clearly show that the Pb-doped $LiCoO_2$ with 5 mol% Pb (Pb5), show much better capacity retention in comparison to pristine $LiCoO_2$. The reason for this improvement must be related to the decreased impedance and stabilization of the layered rhombohedral phase of $LiCoO_2$ due to Pb doping. Pb-doped $LiCoO_2$ with 10 mol% Pb (Pb10) compound shows the decrease in reversible capacity due to cation mixing as discussed in XRD analysis.

Conclusion

Pb-doped $LiCoO_2$ cathode materials are synthesised by combustion synthesis technique. XRD analyses show the highly ordered array of cobalt and oxygen atoms. The layered $LiCoO_2$ structure is retained in the doped samples with an expansion of the lattice. SEM studies revealed an increase in grain size with increase in Pb content. The XPS studies investigated the elementary states on the system. The electrical conductivity of the samples increases with increase in Pb content. The impedance of the fabricated cell with Pb-doped $LiCoO_2$/Li decreases with increase in Pb content. 5 mol% of Pb-doped $LiCoO_2$ has been observed to exhibit a good electrochemical performance particularly less capacity fading in long cycles. This result is attributed to good structure stability of the 5 mol% of Pb-doped $LiCoO_2$ system.

Acknowledgement The authors R. Chandramohan and S. Valanarasu thank the University Grants Commission (UGC-SERO), Hyderabad, India for the financial support for this work.

References

1. Cho J, Kim CS, Yoo SI (2000) Electrochem Solid State Lett 3:362
2. Chen Z, Dahn JR (2002) Electrochem Solid State Lett 5:A213
3. Gabrisch H, Yazami R, Fultz B (2004) J Electrochem Soc 151:A891
4. Xu HY, Xie S, Zhang CP, Chen CH (2005) J Power Sources 148:90
5. Fey GTK, Muralidharan P, Lu CZ, Cho YD (2006) Electrochim Acta 51:4850
6. Lu Z, MacNeil DD, Dahn JR (2001) Electrochem Solid State Lett 4:A200
7. Gopukumar S, Jeong Y, Kim KB (2003) Solid State Ionics 159:223
8. Jones CD, Rossen E, Dahn JR (1994) Solid State Ionics 68:65
9. Julien C, Camacho-Lopez MA, Mohan T, Chitra S, Kalyani P, Gopukumar S (2000) Solid State Ionics 135:241
10. Sadoune I, Delmas C (1998) J Solid State Chem 136:8
11. Kobayashi H, Shigemura S, Tabuchi M, Sakaebe H, Ado K, Kageyama H, Hirano A, Kanno R, Wakita M, Morimoto S, Nasu S (2000) J Electrochem Soc 147:960
12. Zou M, Yoshio M, Gopukumar S, Yamaki JI (2003) Chem Mater 15:4699
13. Zou M, Yoshio M, Gopukumar S, Yamaki JI (2005) Chem Mater 17:1284
14. Needham SA, Wang GX, Liu HK, Drozd VA, Liu RS (2007) J Power Sources 174:828
15. Lukavsky J, Furnadjieva S, Cepak V (2003) Archiv für Hydrobiologie. Supplementband, Algological studies 149
16. Motohashi T, Nakayama Y, Fujita T, Kitazawa K, Shimoyama J, Kishio K (1999) Phys Rev B 59:14080
17. Ghosh P, Mahanty S, Basu RN (2008) Electrochim Acta 54:1654
18. Kalyani P, Kalaiselvi N, Muniyandi N (2002) Mater Chem Phys 77:662
19. Lee T, Cho K, Oh J, Shin D (2007) J Power Sources 174:394

20. Alcantara R, Oritz GF, Lavela P, Tirado JL, Jaegermann W, Thiben A (2005) J Electroanal Chem 584:147
21. Rahmana MM, Krishnab KM, Sogac T, Jimboc T, Umenoa M (1999) J Phys Chem Solids 60:201
22. Huang S, Wen Z, Yang X, Gu Z, Xu X (2005) J Power Sources 148:72
23. Ghosh P, Mahanty S, Basu RN (2008) Mater Chem Phys 110:406
24. Chen CH, Liu J, Amine K (2001) J Power Sources 96:321